Deflection of 400 GeV/c proton beam with bent silicon crystals at the CERN Super Proton Synchrotron

Walter Scandale
CERN, European Organization for Nuclear Research, CH-1211 Geneva 23, Switzerland

Alberto Carnera,[1,2] Gianantonio Della Mea,[1,3] Davide De Salvador,[1,2] Riccardo Milan,[1] and Alberto Vomiero[1,4]
[1]*INFN Laboratori Nazionali di Legnaro, Viale Università 2, 35020 Legnaro (PD), Italy*
[2]*Dipartimento di Fisica, Università di Padova, Via Marzolo 8, 35131 Padova, Italy*
[3]*Dipartimento di Ingegneria dei Materiali e Tecnologie Industriali, Università di Trento, Via Mesiano 77, 38050 Trento, Italy*
[4]*INFM-CNR, Via Valotti 9, 25133 Brescia, Italy*

Stefano Baricordi, Pietro Dalpiaz, Massimiliano Fiorini, Vincenzo Guidi, Giuliano Martinelli, Andrea Mazzolari, and Emiliano Milan
INFN Sezione di Ferrara, Dipartimento di Fisica, and Università di Ferrara Via Saragat 1, 44100 Ferrara, Italy

Giovanni Ambrosi, Philipp Azzarello, Roberto Battiston, Bruna Bertucci, William J. Burger, Maria Ionica, and Paolo Zuccon
INFN Sezione di Perugia and Università degli Studi di Perugia, Dipartimento di Fisica Via Pascoli, 06123 Perugia, Italy

Gianluca Cavoto, Roberta Santacesaria, and Paolo Valente
INFN Sezione di Roma, Piazzale Aldo Moro 2, 00185 Rome, Italy

Erik Vallazza
INFN Sezione di Trieste, Via Valerio 2, 34127 Trieste, Italy

Alexander G. Afonin, Vladimir T. Baranov, Yury A. Chesnokov, Vladilen I. Kotov, Vladimir A. Maisheev, and Igor A. Yazynin
Institute of High Energy Physics, Moscow Region, RU-142284 Protvino. Russia

Sergey V. Afanasiev, Alexander D. Kovalenko, and Alexander M. Taratin
Joint Institute for Nuclear Research, Joliot-Curie 6, 141980, Dubna, Moscow Region, Russia

Alexander S. Denisov, Yury A. Gavrikov, Yuri M. Ivanov, Vladimir G. Ivochkin, Sergey V. Kosyanenko, Anatoli A. Petrunin, Vyacheslav V. Skorobogatov, and Vsevolod M. Suvorov
Petersburg Nuclear Physics Institute, 188300 Gatchina, Leningrad Region, Russia

Davide Bolognini, Luca Foggetta, Said Hasan, and Michela Prest
Università dell'Insubria, via Valleggio 11, 22100 Como, and INFN Sezione di Milano Bicocca, Piazza della Scienza 3, 20126 Milan, Italy
(Received 10 October 2007; published 11 June 2008)

This paper presents a detailed study of the deflection phenomena of a 400 GeV/c proton beam impinging on a new generation of bent silicon crystals; the tests have been performed at the CERN Super Proton Synchrotron H8 beam line. Channeling and volume reflection angles are measured with an extremely precise goniometer and with high resolution silicon microstrip detectors. Volume reflection has been observed and measured for the first time at this energy, with a single-pass efficiency as large as 98%, in good agreement with the simulation results. This efficiency makes volume reflection a possible candidate for collimation with bent crystals at the CERN Large Hadron Collider.

DOI: 10.1103/PhysRevSTAB.11.063501 PACS numbers: 29.27.−a, 42.79.Ag, 61.85.+p

I. INTRODUCTION

Channeling [1] is the confinement between crystalline planes occurring when particles hit a crystal with a momentum nearly parallel to the atomic planes and a transverse kinetic energy not exceeding the well depth U_0 of the crystal potential $U(x)$ averaged over the crystallographic planes [Figs. 1(a) and 1(c)].

When a particle enters a stable channeling condition (i.e. it has a negligible probability of dechanneling as in the short crystals used in this data taking), the critical angle

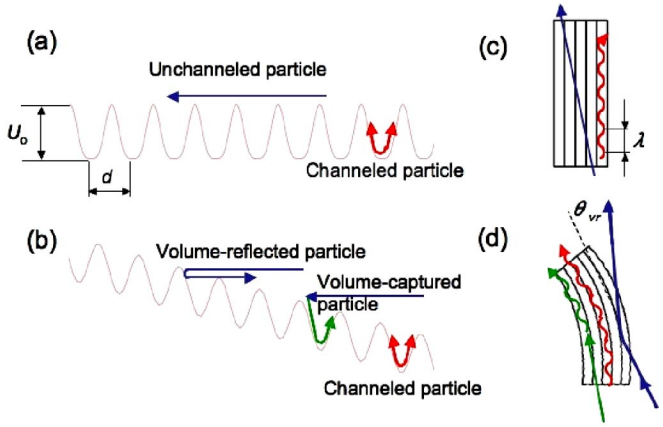

FIG. 1. (Color) (a) Periodic planar potential in a straight crystal for positively charged particles. The arrows show a channeled particle which oscillates in the potential well and a nonchanneled particle, whose transverse energy is greater than the depth of the potential well U_0. (c) Schematic representation of the particle trajectories in a straight crystal. (b) Periodic planar potential in a bent crystal for positively charged particles. The arrows show volume reflected, volume captured, and channeled particles. (d) Schematic representation of the particle trajectories in a bent crystal. Typical values for a (110) crystal are $U_0 = 22.7$ eV, $d = 0.192$ nm.

$\theta_{cs} = \sqrt{\frac{2E_{xc}}{E}}$ is determined by the critical transverse energy $E_{xc} = U(x_c)$, where x_c is the distance at which the probability of nuclear scattering becomes relevant. The upper limit on θ_{cs} is given by $\theta_C = \sqrt{\frac{2U_0}{E}}$. In a bent crystal, a centrifugal term proportional to the curvature generates a linear contribution across the planes which reduces the depth of the potential well. For moderate bending, the interplanar potential wells are preserved and the channeling remains effective [see Fig. 1(b)]; a channeled particle oscillates following the curvature, reaching a final deflection angle of l/R, where l is the crystal length and R the curvature radius. The smallest R that allows channeling is $R_C = E/eE_m$, where E_m is the maximum strength of the planar electric field [2,3]. $E_m \approx 6$ GV/cm for (110) silicon gives $R_C = 68$ cm for 400 GeV/c protons.

In (111) silicon crystals the depth of the potential well is $U_0 = 25$ eV and the interplanar spacing $d = 0.235$ nm, while in (110) silicon crystals $U_0 = 22.7$ eV and $d = 0.192$ nm. θ_C is therefore about 10 μrad for 400 GeV/c protons on silicon.

The deflection of channeled particles in bent crystals was intensively studied at circular accelerators. The record extraction efficiency of 85% has been obtained with a 70 GeV proton beam at the Institute for High Energy Physics (IHEP) accelerator with a bent silicon crystal thanks to the multiturn effect [4].

A particle, which is not aligned with a channel at the crystal entry face but moves toward the curvature center, proceeds along the bent crystal planes until its momentum direction becomes nearly tangent to one of them. Here two effects may take place [Fig. 1(b)]: either the particle partially loses its transverse energy and gets trapped into the channel (*volume capture*) [5,6] or its transverse direction is elastically reversed by interaction with the potential barrier (*volume reflection*) [7,8]. In this second case, there are two parts (branches) of the particle trajectory, one approaching to and another moving away from the tangency point with the angular deflection occurring in both branches.

Volume capture scales with the particle energy approximately as $E^{-3/2}$ and thereby is less probable at high energies where volume reflection (VR) becomes the dominant effect. Almost all particles are then subject to volume reflection, resulting in a transverse kick that deflects them externally with respect to the center of curvature of the crystalline planes [Fig. 1(d)]. Numerical simulations predict that relativistic protons interacting with a bent silicon crystal may be reflected with a deflection angle up to $1.5\theta_C$ for $R \gg R_C$.

Channeling in bent crystals is sometimes used in circular accelerators for beam steering [9], extraction, and collimation [10–12], as well as for splitting and focusing [13] of external beams. Besides, there are on-going investigations to manufacture crystalline undulators [14] and to use bent crystals for measuring the magnetic moments of short-lived particles [15]. In these applications, limitations arise from the small channeling probability. The use of bent crystals as primary collimators for halo collimation in hadron colliders has already been proposed [16–18] and recently demonstrated at the Tevatron collider [19]. A primary collimator should efficiently deflect halo particles towards a downstream massive absorber. While an amorphous target scatters the beam halo over the whole solid angle, a bent crystal deflects halo particles in a given direction, with an angle which can be as large as 20 μrad for 7 TeV protons. This allows one to position the secondary collimator farther from the beam core, reducing impedance, limiting the constraints on its alignment, and avoiding the formation of a tertiary halo. Moreover, volume reflection, given its high efficiency as reported in [20] and described in detail below, is a possible alternative to channeling for collimation.

This paper describes the analysis of the data collected by the H8-RD22 collaboration at the H8 external line of the CERN Super Proton Synchrotron (SPS) with 400 GeV/c protons interacting with different types of bent silicon crystals. Deflection angles of the order of 100 μrad due to channeling and of the order of 10 μrad due to volume reflection are reported and the measurements of the corresponding probabilities are given and compared with simulation.

II. EXPERIMENTAL SETUP

The study of particle deflection phenomena on bent crystals requires a particle beam with an extremely low

TABLE I. Parameters of the bent silicon crystals tested during the data-taking period. The lattice orientation is specified in parentheses. The length (L) is measured along the z-axis, the width (W) along x, and the height (H) along y (given in mm). The measured deflection angles due to channeling are given in μrad.

Crystal	L	W	H	$\theta_{ch}^{max} - \theta_{un}$
ST4 (110)	3.0	0.9	70	$-162.0 \pm 0.1 \pm 1.1$
QM2 (111)	0.84	30	58	$-68.6 \pm 0.2 \pm 0.9$
ST1 (111)	3.0	0.9	70	$-278.2 \pm 0.8 \pm 3.2$
ST2 (111)	1.85	0.5	70	$-213.6 \pm 3.5 \pm 5.2$
QM1 (111)	0.93	30	58	$-78.1 \pm 4.0 \pm 2.8$

divergence, a high resolution telescope to track particles upstream and downstream the crystal and a high precision goniometer to align the crystals with a high degree of repeatability (of about 1 μrad). Two different types of bent crystals have been manufactured and used in the experiment: strip and quasimosaic crystals.

A. Bent silicon crystal

Silicon strips (in the following indicated with ST1, ST2, and ST4) have been manufactured at the Sensors and Semiconductors Laboratory at Università di Ferrara in collaboration with IHEP [21]. Prime materials are (110) and (111) oriented 4 inch silicon wafers. After a standard cleaning procedure, the wafer is diced to a strip size (whose dimensions are given in Table I). The crystal is then mounted on a specifically designed holder, which is routinely used at IHEP for beam extraction [22]. The holder bends the crystal primarily around an axis parallel to the beam direction, generating anticlastic forces which give rise to a secondary curvature around the vertical axis so that the proton beam is deflected horizontally (Fig. 2).

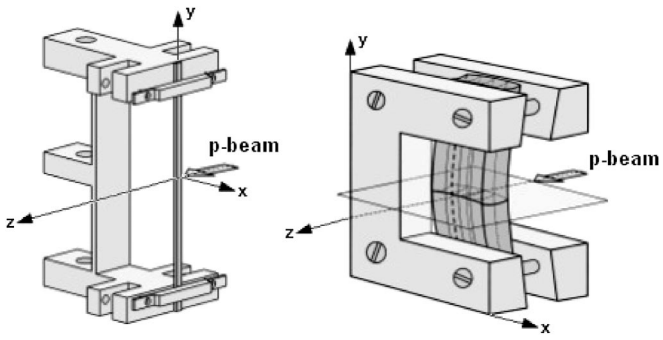

FIG. 2. Schematic drawings of the crystal holders for a strip (left) and a quasimosaic (right). The crystal dimensions are given in Table I.

The second type of crystals (in the following indicated as QM1 and QM2) has been prepared exploiting the elastic-quasimosaicity effect at the Petersburg Nuclear Physics Institute [23]. The crystal plate sizes are given in Table I with the (111) channeling planes parallel to the yz face.

B. Apparatus layout

The experimental layout is illustrated in Fig. 3 where the various elements are drawn with their longitudinal position along the beam direction. The apparatus is organized in two areas: the one with the crystal assembled on the goniometer and the "far detector area" located 60 m downstream with respect to the crystal to allow the measurement of the crystal effects with the available detectors. More details are given in [24].

The crystals are mounted on mechanical holders (Fig. 2), fixed on a remotely controlled goniometer system (G in Fig. 3). In order to improve the mechanical stability of the goniometer, the whole system is installed on a precisely machined granite table and the relative position of the goniometer is determined with a laser. Each crystal is aligned with respect to the beam with an "angular scan" around a vertical axis, while a linear motor allows one to extract the crystal from the beam to measure the beam characteristics (profile and divergence). The most demanding feature of the goniometric system is the repeatability of the alignment process (1.0 μrad).

The basic idea of the experiment is to track every single particle that crosses the crystal and to determine the single-pass efficiency of the beam deflection due either to channeling or to volume reflection.

The tracking system consists of two independent silicon microstrip setups with an excellent spatial resolution, and a fast parallel-plate gas chamber; scintillation counters were used for the trigger. The two silicon tracking setups were based on two different types of detectors, the AMS-type [25] ($41 \times 72 \times 0.3$) mm^3 double-sided silicon microstrip sensors (110 μm and 208 μm readout pitch, 8.5 μm and 30 μm resolution for the p- and n-sides, respectively), and the AGILE-type [26] 410 μm thick, (9.5×9.5) cm^2 single-sided (but each module is composed of two detectors in order to have a x-y measurement) silicon microstrip

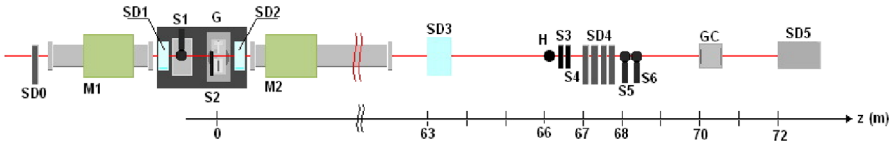

FIG. 3. (Color) Schematic drawing of the experimental layout. The longitudinal positions of the various elements whose symbols are defined in the text are indicated.

detectors (30 μm resolution). Each setup consisted of a detector positioned near the crystal (SD1 and SD2 for the AMS-type, just before and after the crystal on the same granite block and an AGILE-type, SD0, before the first bending magnet) and of a set of detectors located in the far area. The near crystal detectors are used to define the proton impact point on the crystal surface.

In the same region, two scintillation counters could be used to find the exact position of the crystal with respect to the beam: S1 on the granite table which can select a 100 μm thick vertical beam slice and S2 (80 μm thick) assembled on the upper linear stage of the goniometer. Several detection systems in the far area allow one to track the particle: SD3, composed of 4 double-sided AMS-type detectors; a scintillating hodoscope (H), made of 2 mm in diameter 16 scintillating strips, to provide a fast indication on the crystal alignment; a pair of identical scintillators (S3, S4 with a dimension of 10×10 cm^2) downstream the hodoscope, matching exactly the dimension of the AGILE-type silicon detector (SD4), which is installed close to them; SD5, a set of 6 *x-y* AGILE-type modules, for cross-check purposes.

High statistics is needed in a short time for a fast crystal alignment. Since the silicon detectors acquisition rate is limited to a few kHz, a fast parallel-plate position-sensitive gas chamber detector (GC in Fig. 3) is used, which can withstand particle rates up to 10^8 protons-per-pulse (ppp) for a pulse duration of 4.8 s.

C. Data taking

The experiment has been performed on a primary 400 GeV/c proton beam at the CERN SPS H8 external beam line. The beam spot diameter at the crystal has been measured to be about 1 mm. The primary beam intensity (20×10^{11} ppp) has been reduced to about 5×10^4 ppp without significantly affecting its divergence. This intensity is relatively low and allows single particle tracking. The beam had a continuous time structure with a flattop of 4.8 s duration every 16.8 s.

A total of more than 1000 runs were recorded during the data taking, each run corresponding to one crystal angular position (ϕ). For each crystal exposed to the beam a fast prealignment was performed to find the angular position corresponding to the channeling configuration. For this purpose, the beam was switched to the high intensity mode (10^7 ppp) and the beam profiles detected by the gas chamber were inspected online. Because of the clearly visible double peak structure, a few steps were sufficient to find the channeling position. Successively the beam was retuned to the medium intensity mode (10^4 ppp) and high statistics runs were recorded with all the detectors, while varying the goniometer angle (angular scan). In the typical run about 10 k events and 3 k events were taken in one SPS spill for the silicon detectors of the AMS- and AGILE-type, respectively. Usually about 10–15 accelerator cycles were enough to accumulate an adequate statistics for both types of detectors.

III. DATA ANALYSIS

This section describes the data analysis procedure. The angular position of the channeled and volume reflected portion of the beam with respect to the unperturbed beam and the efficiencies of such processes are measured for all the crystals tested during the data taking. Relevant plots are given for ST4 and QM2 crystals as examples while the final results are summarized for all the crystals.

A. Angular scan

The prealignment procedure described in the previous section determined the angular range that has to be covered by the scan for each crystal.

Figure 4 shows an example of a typical high statistics angular scan for the ST4 crystal performed with the silicon detectors after the alignment procedure. The color code indicates the number of tracks at a given lateral x position (vertical axis) of the SD4 detector for various crystal angular positions ϕ (horizontal axis).

The following features can be identified: (i) the ''amorphous'' areas at the beginning and at the end of the scan, which correspond to crystal angles at which the beam goes through the crystal with no perturbation besides the multiple scattering effect (''unperturbed'' beam); (ii) the channeling region ($\phi \sim 65$ μrad) showing a clear accumulation of deflected tracks; (iii) the volume reflection

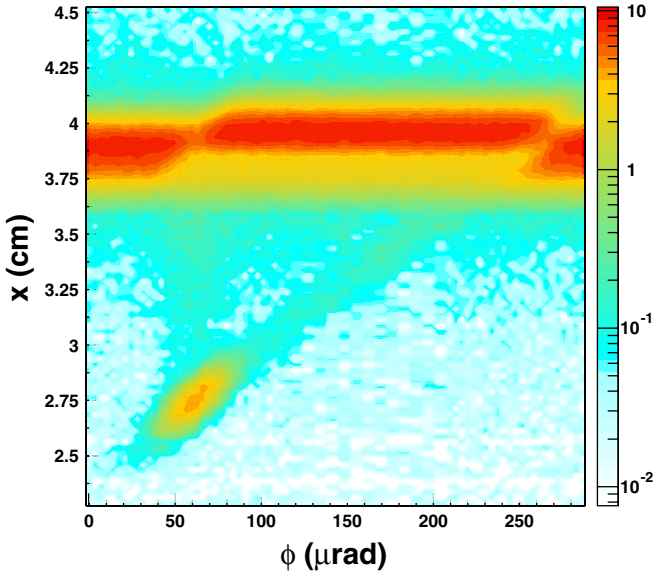

FIG. 4. (Color) Angular scan of the ST4 crystal. The color code represents the relative number of tracks at different lateral x positions on the SD4 detector (vertical axis). On the horizontal axis the crystal angle ϕ is reported, corresponding to a different data-taking run (the number of tracks for each run is normalized to the number of triggers in that same run).

region ($70 < \phi < 250$ μrad). It is evident that the volume reflection causes a shift of the proton beam to the opposite direction with respect to channeling. While such a shift is smaller than the channeling one, it occurs for a much wider angular range and with a higher probability. The faint vertical band in the channeling region corresponds to the *dechanneling* phenomenon due to the particles which start to be channeled at the entry face of the crystal but exit before reaching the end of the crystal. In the volume reflection region, a diagonal low intensity band corresponds to the *volume capture* occurring when particles, initially not channeled, due to multiple scattering on the nuclei of the crystal, get trapped between the lattice planes at an intermediate position along the crystal length and are therefore only partially deflected.

B. Particle angle measurements

Although the main features of the phenomena under study are clearly visible in Fig. 4, a detailed data analysis was performed to improve the measurement precision.

A selection was applied to the silicon detectors raw data in order to eliminate dead and noisy strips determined with a calibration procedure. Position measurements were separately performed on the two views of the silicon detectors. The cluster position was identified with a charge-weight algorithm applied on adjacent strips with a signal above threshold. Events with more than one cluster per view were rejected. The relative alignment of the detector planes was performed by using dedicated runs with no crystal.

The particle trajectory after the interaction with the crystal is obtained measuring the *particle angle* θ. Given that the beam divergence is small (thus the particles are in practice parallel), the particle position at the entry face of the crystal is determined by the upstream detector SD0 (SD1) and the angle θ can be found joining the x coordinate measured by SD0 (SD1) with the one measured by SD4 (SD3). The angular distribution of the unperturbed beam component [Fig. 5(a)] has a rms of 8.57 μrad. From a careful survey of the material present along the beam line, the contribution due to multiple scattering has been estimated to be 3.46 ± 0.03 μrad with a Monte Carlo simulation based on GEANT4 [27]. This results in a beam divergence at the crystal of 7.84 ± 0.07 μrad. The θ definition therefore allows one to take into account the finite dimension of the beam spot at the crystal.

It has to be noticed that, since for each type of silicon detector only one x-y plane is available upstream the crystal, it is not possible to reconstruct the angle of the particle entering the crystal.

The SD0 and SD1 detectors have been used also to discard particles not crossing the crystal thus selecting a fiducial area.

The events shown in the scan summary plot in Fig. 6, obtained with the θ angle reconstruction and selecting the particles hitting the central part of the crystal, are the basis for further analysis.

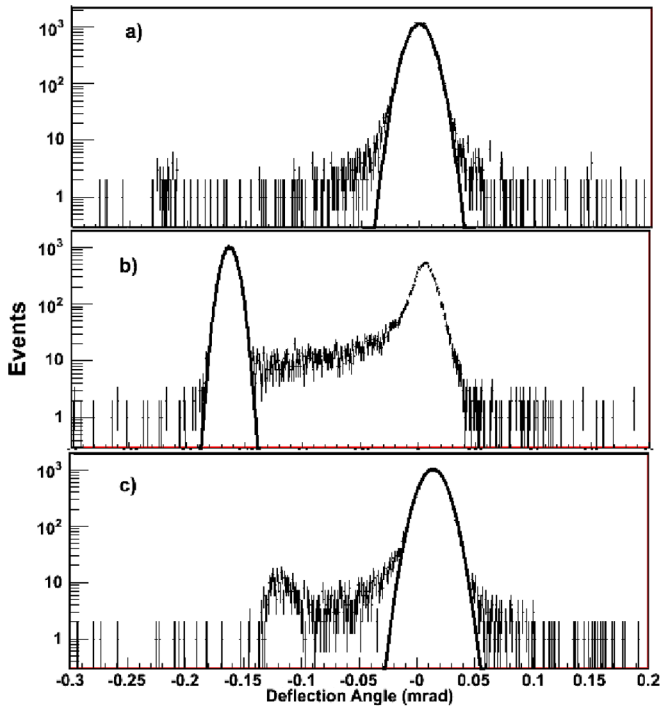

FIG. 5. (Color) Beam profiles for the ST4 crystal in different crystal positions with a superimposed Gaussian fit: (a) amorphous region (at the beginning and at the end of the scan in Fig. 4), (b) channeling region ($\phi \sim 65$ μrad in Fig. 4), (c) volume reflection region ($70 < \phi < 250$ μrad in Fig. 4).

In the case of the QM2 crystal the fraction of particles not crossing the crystal is negligible, as expected, since this crystal has a much larger cross section with respect to the beam spot. Figure 7 shows the angular scan summary plot for the QM2 crystal.

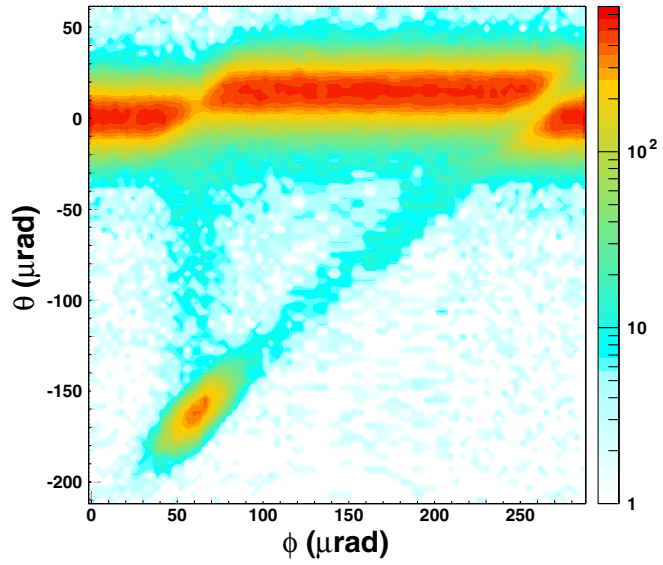

FIG. 6. (Color) Angular scan of the ST4 crystal selecting only the middle horizontal part of the beam. On the horizontal axis the crystal rotation angle; on the vertical axis the particle angle.

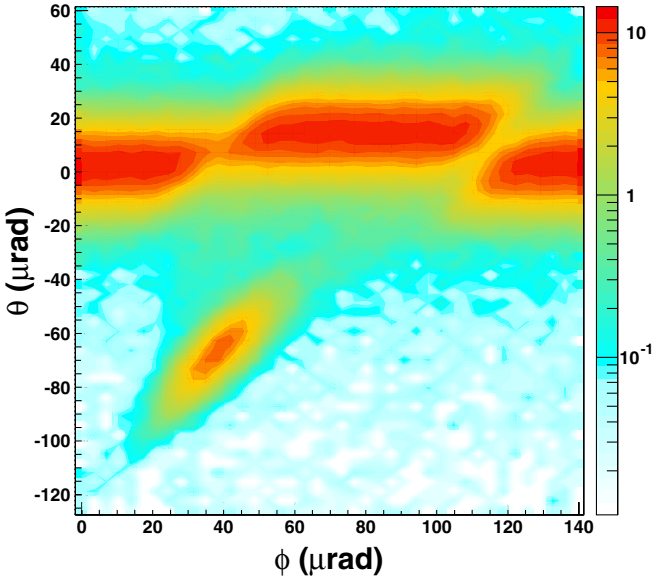

FIG. 7. (Color) Angular scan of the QM2 crystal. On the horizontal axis the crystal rotation angle; on the vertical axis the particle angle.

C. Deflection angles measurement

The θ distributions for three orientations of the ST4 crystals are shown in Fig. 5 as an example. The orientations correspond to an amorphous position (a), the position of the best alignment for channeling (b), and a middle position within the volume reflection region (c). The value of the peak position and the width of the distribution for the unperturbed (θ_{un}, σ_{un}), channeling (θ_{ch}, σ_{ch}), and volume reflection (θ_{vr}, σ_{vr}) portions of the beam are then extracted with a fit, using a Gaussian parametrization for each component.

The *channeling deflection angle* is defined as the difference $\theta_{ch}^{max} - \theta_{un}$. θ_{un} is estimated from an average in the runs with the crystal in an amorphous position. To find θ_{ch}^{max}, ϕ_{max} (corresponding to the position of perfect alignment of the crystal with respect to the beam) has to be computed. This is accomplished performing a Gaussian fit to the fraction of tracks in the channeled beam in the channeling angular range, as shown in Fig. 8. A linear relation between θ_{ch} and ϕ is derived in this same angular range as shown in Fig. 9. θ_{ch}^{max} corresponding to ϕ_{max} is then computed from this relation.

Following the same procedure for the volume reflection, the *deflection angle at volume reflection* is defined as $\theta_{vr} - \theta_{un}$. In this case θ_{vr} is determined as an average over the peak positions in the crystal angular range $\Delta\phi_{vr}$ defined as the length of the basis of the parallelogram including the volume reflection region (visible in the angular scans in Fig. 6 and in Fig. 7).

The results of these measurements are given in Tables I and II for the various crystals.

A more complex parametrization of the θ distributions with more Gaussian components in the fit is used to estimate the presence of secondary components in the unperturbed beam and of the less probable effects (dechanneling, volume capture). The dependence on ϕ of $\theta_{vr} - \theta_{un}$ is ascribed to the same modeling assumption. This effect translates into a 4% relative systematic error (the largest component of the error itself) on the $\theta_{vr} - \theta_{un}$. The relative uncertainty on the distance between the crystal and the SD4 (SD3) detector is 10^{-4} being thus negligible as far as the measurements of θ is concerned. Residual effects of misalignment of the detectors are evaluated to be negligible as well.

The systematic error takes into account both torsional effects (as described in the next subsection) and small crystal nonuniformities in x and y which translate in the dependence of the measured θ from x and y.

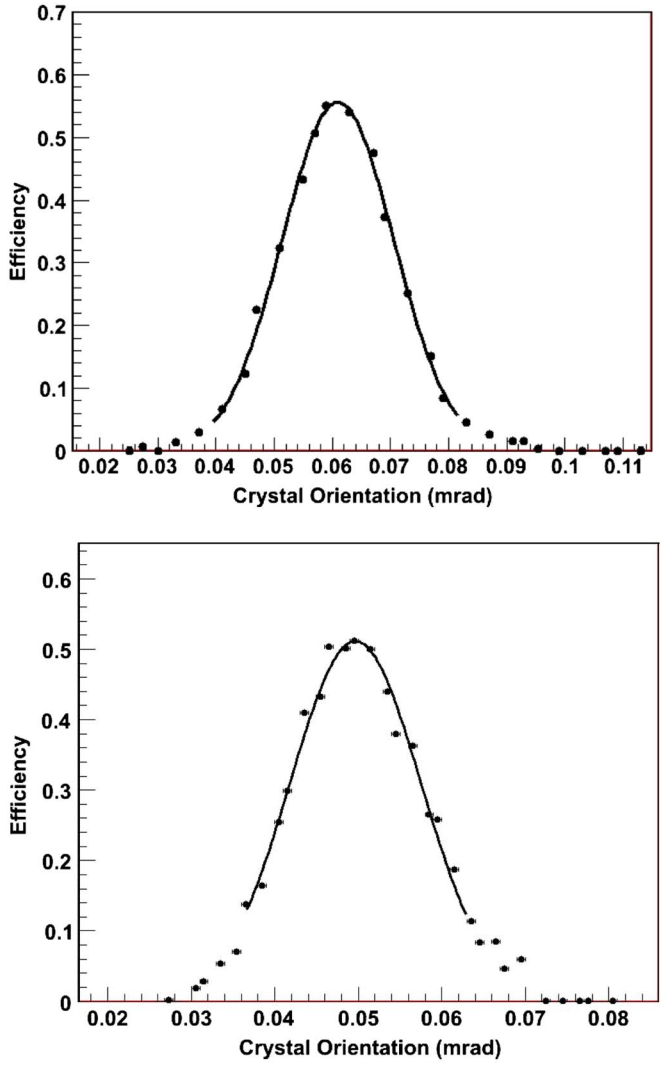

FIG. 8. (Color) Fraction of protons in the channeled beam component for the ST4 (upper) and the QM2 (lower) crystal as a function of the crystal angle (ϕ). From a Gaussian fit to this distribution the crystal orientation of maximal channeling probability, ϕ_{max}, and the probability (Sec. III D) itself, P_{ch}, are computed.

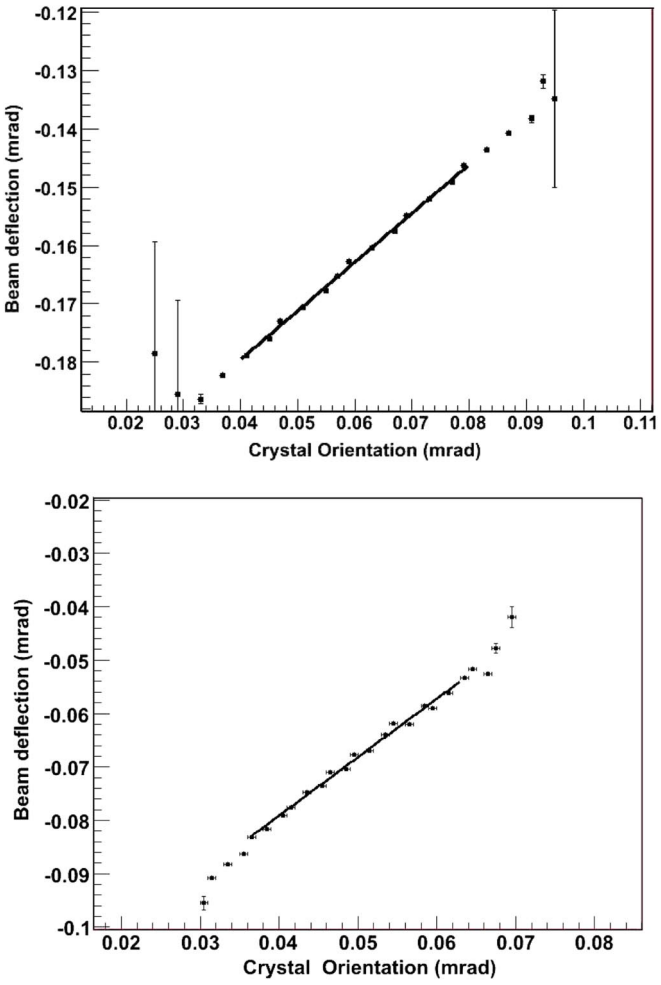

FIG. 9. (Color) Beam deflection θ_{ch} as a function of the crystal angle position, with a linear fit superimposed for ST4 (upper) and QM2 (lower). This linear fit is used to convert the crystal angle position of maximal channeling into θ_{ch}^{max}.

D. Efficiencies measurements

The various phenomena of particle deflection are characterized by a probability (''efficiency'') that can be computed from the data comparing the fraction of particles in the various regions of the angular scan.

To determine an appropriate normalization each run of the scan has been normalized to the number of collected triggers $N_{run\phi}$, where ϕ identifies a given crystal angle. The number of protons in the unperturbed beam, N_{un}, is defined as the number of protons within $\pm 3\sigma_{un}$ around θ_{un}.

The channeling efficiency is therefore defined as

$$P_{ch} = \frac{N_{ch}/N_{run\phi_{ch}}}{\langle N_{un}/N_{run\phi_{un}}\rangle}, \quad (1)$$

where N_{ch} is the number of protons within $\pm 3\sigma_{ch}$ around θ_{ch} and the average $\langle N_{un}/N_{run\phi_{un}}\rangle$ is computed over all the explored amorphous positions.

P_{ch} is shown in Fig. 8 as a function of the crystal angle. The maximal P_{ch} for the various crystals are reported in Table II.

The evaluation of the volume reflection efficiency (P_{vr}) has been carried out with two independent methods. Similarly to the channeling case, the protons N_{vr} are counted within $\pm 3\sigma_{vr}$ around θ_{vr}:

$$P_{vr} = \frac{N_{vr}/N_{run\phi_{vr}}}{\langle N_{un}/N_{run\phi_{un}}\rangle}. \quad (2)$$

In Fig. 10 the P_{vr} values are shown as a function of the crystal angle. The mean values of P_{vr} (averaged over the volume reflection region) for all the crystals are given in Table II.

As far as the second method to compute P_{vr} is concerned, referring to Fig. 6 the fraction of events in the beam tail with the crystal in the amorphous positions ($\theta > \theta_{un} + 3\sigma_{un}$) is subtracted from the fraction of events in the volume reflection region with $\theta > \theta_{vr} + 3\sigma_{vr}$. This remaining part is due to the volume capture and to other inefficiencies. This method gives results completely consistent with the ones of the first method and it is used to measure the other less probable effects.

The volume capture contribution (P_{vc}) is in fact estimated in the same volume reflection region by counting the events in the diagonal area (Fig. 6). The volume capture peak is fitted with a Gaussian function for each crystal position and events are counted within 3σ and background subtracted. The average value for P_{vc} is $(1.28 \pm 0.06)\%$ and $(2.21 \pm 0.16)\%$ for ST4 and QM2, respectively, where the error is statistical only. The dechanneling efficiency P_{dch} is extracted for the crystal position corresponding to the maximal P_{ch}. It is estimated from the fraction of events with $\theta_{vr} + 3\sigma_{vr} < \theta < \theta_{ch} - 3\sigma_{ch}$ having subtracted the background events counted in the tails of the beam in the amorphous positions and results to be $(4.56 \pm 0.43)\%$ and $(1.42 \pm 0.39)\%$ for ST4 and QM2, respectively, where the error is statistical only.

The definitions of the number of events N_j rely on the Gaussian assumption for the shape of the beam distributions. To estimate the systematic uncertainty due to this assumption, the efficiency has been computed using a different number of σ to calculate N_j and the stability of the measurement as a function of ϕ has been checked. This turns out to be the dominant component of the error on the efficiencies as reported in Table II.

In Fig. 11 the particle angle distribution is shown as a function of the vertical particle position at SD0. Though only a small vertical part of the beam seems not to be deflected, a dependence of the channeling deflection angle on the particle vertical position is evident. This is interpreted as a significant indication of a crystal torsion, that is measured to be $\delta = 10.7 \pm 0.1$ μrad/mm for the ST4 crystal and 3.3 ± 0.1 μrad/cm for the QM2 crystal.

TABLE II. Results on the volume reflection deflection angles (in μrad), channeling efficiency, and volume reflection efficiency for the various tested crystals. Statistical errors from the fit and systematic errors are given. The values obtained from the simulation are reported for each crystal (in the second line). Their relative error is dominated by the model uncertainty (15%).

Crystal	Maximal P_{ch} (%)	$\theta_{\mathrm{vr}} - \theta_{\mathrm{un}}$	$\langle P_{vr} \rangle$ (%)
ST4	$56.2 \pm 0.5 \pm 2.0$	$13.91 \pm 0.03 \pm 0.50$	$98.17 \pm 0.04 \pm 0.50$
	53	15	97
QM2	$51.9 \pm 0.3 \pm 2.1$	$11.70 \pm 0.02 \pm 0.51$	$98.27 \pm 0.04 \pm 0.50$
	50	13	97
ST1	$38.5 \pm 0.2 \pm 2.7$	$10.45 \pm 0.04 \pm 0.47$	$98.31 \pm 0.04 \pm 0.50$
	45	13	98
ST2	$43.6 \pm 0.3 \pm 7.3$	$11.10 \pm 0.05 \pm 0.54$	$98.40 \pm 0.60 \pm 0.50$
	45	12	98
QM1	$41.3 \pm 0.4 \pm 7.1$	$11.90 \pm 0.04 \pm 0.59$	$97.80 \pm 0.40 \pm 0.50$
	50	13	98

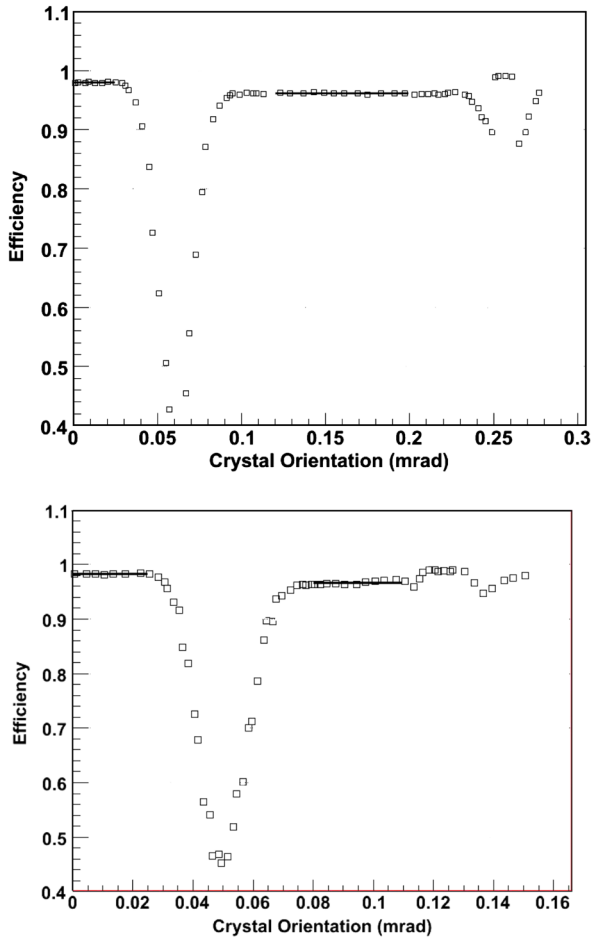

FIG. 10. (Color) Fraction of protons in the main beam component as a function of the crystal angle; crystal angles around 0 correspond to the amorphous position. At each crystal angle, the total number of events is equalized to $N_{\mathrm{run}\phi}$. Top plot: ST4, bottom plot: QM2.

IV. COMPARISONS WITH THEORETICAL EXPECTATIONS

Particle trajectories in a bent crystal were calculated using the effective potential of bent atomic planes according to the model of Planar Channeling in a Bent Crystal (PCinBC), which was developed in [6]. The description of the model can be found in [2].

The change of the particle direction due to multiple scattering on the crystal nuclei was calculated after its passage through a crystal layer whose thickness is much smaller than the wavelength of the particle oscillations in the planar channel. The inelastic nuclear interactions of protons in the crystals were included.

Figure 12 shows the predicted angular distribution of 400 GeV/c protons which cross the QM2 crystal. It is assumed that the incident beam has a Gaussian angular distribution with $\sigma = 8$ μrad, which is similar to the H8 beam.

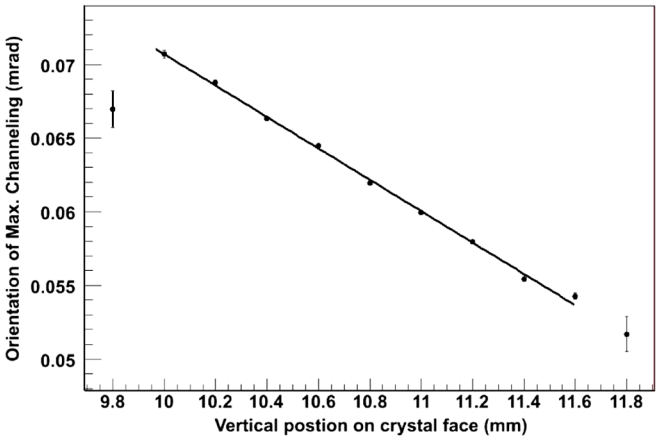

FIG. 11. Angle of maximal channeling versus the proton vertical position for the ST4 crystal. The shifting of $\theta_{\mathrm{ch}}^{\mathrm{max}}$ is interpreted as due to a torsion of the crystal.

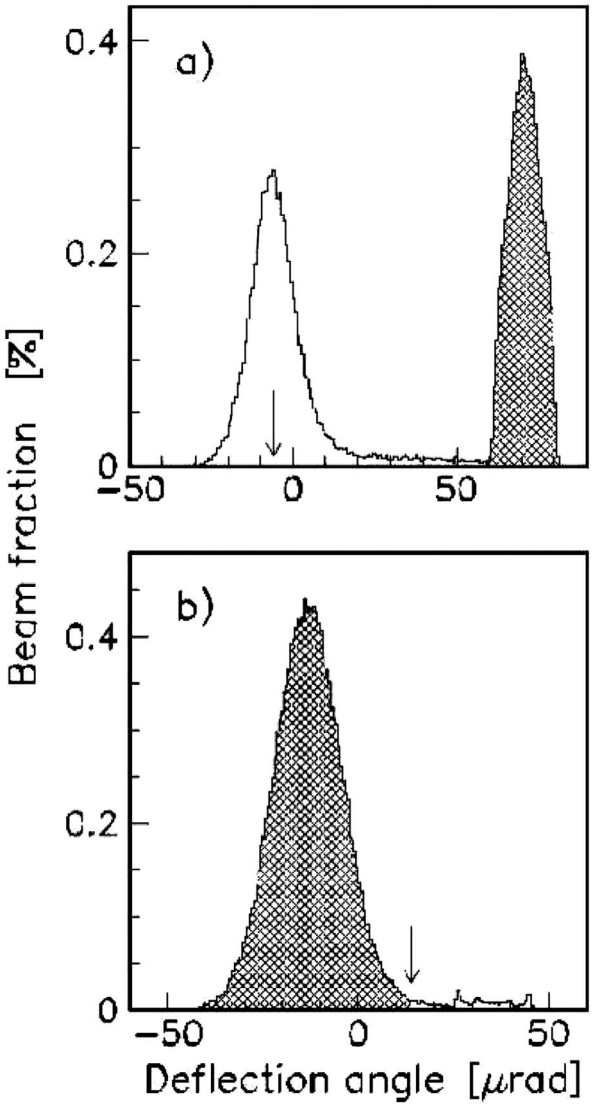

FIG. 12. Calculated angular distributions of 400 GeV/c protons after crossing the QM2 crystal. (a) For a perfect alignment, $\phi_{\max} = 0$; the channeled beam fraction is indicated by the hatched area. The arrow shows the deflection angle of the nonchanneled beam portion. (b) For the case of volume reflection, $\phi = 35.5$ μrad; the reflected beam portion is hatched. The arrow shows the boundary of the reflected portion (the angle $\theta_{vr} + 3\sigma_{vr}$). The angular deflection is positive with respect to the crystal bending (opposite to the experimental distributions).

The distribution shown in Fig. 12 considers a perfect alignment between the bent plane direction at the crystal entrance and the beam axis ($\phi_{\max} = 0$), in which case the capture of protons into the channeling regime is maximal. The beam part channeled through the whole crystal is deflected by the crystal bending angle [hatched in Fig. 12(a)]. The channeling deflection efficiency is $P_{ch} = 50.4\%$. The full width of the channeled peak is about 20 μrad, which is close to $2\theta_C$. The nonchanneled beam part is reflected by the planar potential. The volume reflection deflection angle is $\theta_{vr} = 6.1$ μrad because there is only one of the two branches of the reflection trajectory in this case (particles have the tangency point near the crystal entrance). Figure 12(b) shows the calculated angular distribution of protons in the case of volume reflection at the crystal angle $\phi = 35.5$ μrad when the tangency point of the beam axis to the bent planes is in the middle of the crystal. The reflected beam maximum is at $\theta_{vr} = 13.12$ μrad and $\sigma_{vr} = 9.05$ μrad. The efficiency of volume reflection is determined in the same way of the experimental data and results to be $P_{vr} = 97.2\%$.

The simulation results are characterized by statistical and model uncertainties. The statistical errors for the channeling and VR parameters (deflection angle and efficiency) are smaller than 1%. The model errors are due to the accuracy of the Moliere approximation, which was used for the silicon atomic potential. The Moliere approximation uncertainty for silicon is smaller than 15% according to the x-ray scattering studies.

The simulation was also performed for the other crystals. The results are presented in Table II together with the experimental results. While on one hand, there is a good agreement between the data and simulation for the VR efficiency and the discrepancies for the VR deflection angles are smaller than 15%, on the other the discrepancies for the channeling deflection efficiency are larger, up to 20%. This is caused by a strong dependence of the values on the shape of the angular distribution of the beam (the experimental angular distribution differs from the Gaussian approximation used for the simulation).

V. CONCLUSIONS

The 400 GeV/c proton beam deflection on various bent silicon crystals of about 13 μrad has been interpreted as due to volume reflection; the measured efficiency is larger than 98%. Experimental results and simulation based on the PCinBC model are in good agreement within errors. Meanwhile, a new experimental program has already been carried out with an improved detector to allow measurements which are independent of the beam divergence. The result presented here indicates volume reflection as a possible alternative to channeling for beam collimation at future hadron colliders, being superior both in terms of efficiency and angular acceptance.

The small deflection angle could be increased thanks to the overall effect of many aligned crystals (multireflection) as already demonstrated by the H8-RD22 collaboration [28].

ACKNOWLEDGMENTS

We gratefully acknowledge support from L. Gatignon, I. Efthymiopoulos, P. Lebrun, S. Myers, A. A. Vorobyev, P. M. Levchenko, A. N. Sisakyan, A. I. Malakhov, N. E. Turin, S. Chiozzi, A. Sambo, E. Boscolo Marchi, A. Papi, V. Postolache, and G. Alberti. We also acknowledge

partial support by the European Community-Research Infrastructure Activity under the FP6 Structuring the European Research Area program (CARE, Contract No. RII3-CT-2003-506395), the INFN NTA-HCCC, the INTAS program and MIUR 2006028442 project, Russian Foundation for Basic Research Grant No. 06-02-16912, RF President Foundation Grant No. SS-3057-2006-2, Program ''Elementary Particle Physics and Fundamental Nuclear Physics'' of the Russian Academy of Sciences.

[1] S. Gemmell, Rev. Mod. Phys. **46**, 129 (1974).
[2] A. M. Taratin, Phys. Part. Nucl. **29**, 437 (1998).
[3] V. A. Maisheev, Phys. Rev. ST Accel. Beams **10**, 084701 (2007); A. M. Taratin and W. Scandale, Nucl. Instrum. Methods Phys. Res., Sect. B **262**, 340 (2007).
[4] A. G. Afonin *et al.*, JETP Lett. **74**, 55 (2001).
[5] V. A. Andreev *et al.*, Pis'ma Zh. Eksp. Teor. Fiz. **36**, 340 (1982) [JETP Lett. **36**, 415 (1982)].
[6] A. M. Taratin and S. A. Vorob'ev, Zh. Tekh. Fiz. **55**, 1598 (1985).
[7] A. M. Taratin and S. A. Vorobiev, Nucl. Instrum. Methods Phys. Res., Sect. B **26**, 512 (1987).
[8] Yu. M. Ivanov *et al.*, Phys. Rev. Lett. **97**, 144801 (2006).
[9] A. F. Elishev *et al.*, Phys. Lett. **88B**, 387 (1979).
[10] A. G. Afonin *et al.*, Phys. Rev. Lett. **87**, 094802 (2001).
[11] R. Carrigan *et al.*, Phys. Rev. ST Accel. Beams **5**, 043501 (2002).
[12] R. P. Fliller, III *et al.*, Nucl. Instrum. Methods Phys. Res., Sect. B **234**, 47 (2005).
[13] A. S. Denisov *et al.*, Nucl. Instrum. Methods Phys. Res., Sect. B **69**, 382 (1992).
[14] S. Bellucci *et al.*, Phys. Rev. Lett. **90**, 034801 (2003).
[15] V. V. Baublis *et al.*, Nucl. Instrum. Methods Phys. Res., Sect. B **90**, 112 (1994).
[16] M. A. Maslov *et al.*, Report No. SSCL-484, 1991.
[17] E. Tsyganov and A. Taratin, Nucl. Instrum. Methods Phys. Res., Sect. A **363**, 511 (1995).
[18] V. M. Biryukov *et al.*, Nucl. Instrum. Methods Phys. Res., Sect. B **234**, 23 (2005).
[19] R. Carrigan *et al.*, Proc. SPIE Int. Soc. Opt. Eng. **6634**, 66340I (2007).
[20] W. Scandale *et al.*, Phys. Rev. Lett. **98**, 154801 (2007); W. Scandale, Report No. CARE-Conf-07-017-HHH, 2007.
[21] V. Guidi *et al.*, Nucl. Instrum. Methods Phys. Res., Sect. B **234**, 40 (2005).
[22] A. G. Afonin *et al.*, JETP Lett. **67**, 781 (1998).
[23] Yu. M. Ivanov *et al.*, JETP Lett. **81**, 99 (2005).
[24] W. Scandale *et al.*, Rev. Sci. Instrum. **79**, 023303 (2008).
[25] B. Alpat *et al.*, Nucl. Instrum. Methods Phys. Res., Sect. A **439**, 53 (2000).
[26] M. Prest *et al.*, Nucl. Instrum. Methods Phys. Res., Sect. A **501**, 280 (2003).
[27] S. Agostinelli *et al.*, Nucl. Instrum. Methods Phys. Res., Sect. A **506**, 250 (2003).
[28] W. Scandale *et al.*, Phys. Lett. B **658**, 109 (2008).